Physics of the Earth and Planetary Interiors 260 (2016) 62–73

Contents lists available at ScienceDirect

Physics of the Earth and Planetary Interiors

journal homepage: www.elsevier.com/locate/pepi

Microwave paleointensities indicate a low paleomagnetic dipole moment at the Permo-Triassic boundary

Taslima Anwar [a,*], Louise Hawkins [b], Vadim A. Kravchinsky [a], Andrew J. Biggin [b], Vladimir E. Pavlov [c,d]

[a] Department of Physics, University of Alberta, Edmonton, Alberta T6G 2E1, Canada
[b] Geomagnetism Laboratory, Oliver Lodge Laboratories, School of Environmental Sciences, University of Liverpool, Liverpool L69 7ZE, UK
[c] Institute of Physics of the Earth, Russian Academy of Sciences, Bolshaya Gruzinskaya st., 10, Moscow 123995, Russia
[d] Kazan (Volga region) Federal University, Kremlevskaya ul. 18, Kazan 420008, Russia

ARTICLE INFO

Article history:
Received 11 June 2016
Received in revised form 20 September 2016
Accepted 23 September 2016
Available online 26 September 2016

Keywords:
Geomagnetic dipole moment
Microwave technique
Paleointensity
Permo-Triassic boundary
Siberian trap basalts

ABSTRACT

The quantity of igneous material comprising the Siberian Traps provides a uniquely excellent opportunity to constrain Earth's paleomagnetic field intensity at the Permo-Triassic boundary. There remains however, a contradiction about the strength of the magnetic field that is exacerbated by the limited number of measurement data. To clarify the geomagnetic field behavior during this time period, for the first time, a microwave paleointensity study has been carried out on the Permo-Triassic flood basalts in order to complement existing datasets obtained using conventional thermal techniques. Samples, which have been dated at ~250 Ma, of the Permo-Triassic trap basalts from the northern extrusive (Maymecha-Kotuy region) and the southeastern intrusive (areas of the Sytikanskaya and Yubileinaya kimberlite pipes) localities on the Siberian platform are investigated. These units have already demonstrated reliable paleomagnetic directions consistent with the retention of a primary remanence. Furthermore, Scanning Electron Microscope analysis confirms the presence of iron oxides likely of primary origin. Microwave Thellier-type paleointensity experiments (IZZI protocol with partial thermoremanent magnetization checks) are performed on 50 samples from 11 sites, of which, 28 samples from 7 sites provide satisfactory paleointensity data. The samples display corresponding distinct directional components, positive pTRM checks and little or no zig-zagging of the Arai or Zijderveld plot, providing evidence to support that the samples are not influenced by lab-induced alteration or multi-domain behavior. The accepted microwave paleointensity results from this study are combined with thermal Thellier-type results from previously published studies to obtain overall estimates for different regions of the Siberian Traps. The mean geomagnetic field intensity obtained from the samples of the northern part is 13.4 ± 12.7 μT (Maymecha-Kotuy region), whereas from the southeastern part is 17.3 ± 16.5 μT (Sytikanskaya kimberlite pipe) and 48.5 ± 7.3 μT (Yubileinaya kimberlite pipe), suggesting that the regional discrepancy is probably due to the insufficient sampling of geomagnetic secular variation, and thus, multiple localities need to be considered to obtain an accurate paleomagnetic dipole moment for this time period. It demonstrates that the overall mean paleointensity of the Siberian Traps is 19.5 ± 13.0 μT which corresponds to a mean virtual dipole moment of $3.2 \pm 1.8 \times 10^{22}$ Am^2. Results indicate that the average magnetic field intensity during Permo-Triassic boundary is significantly lower (by approximately 50%) than the present geomagnetic field intensity, and thus, it implies that the Mesozoic dipole low might extend 50 Myr further back in time than previously recognized.

1. Introduction

The behavior of Earth's magnetic field in the geological past is found to be inconsistent and poorly studied for some epochs. Interpreting the changes in the absolute paleointensity variations presents an opportunity to understand the evolution of Earth's magnetic field and to obtain new information about the geodynamo's behavior. It can inform us how the convection in the lowermost part of the Earth's mantle might be influencing the generation of the magnetic field in the underlying core (Valet, 2003; Tauxe and Yamazaki, 2007; Biggin et al., 2012). Reliable absolute geomagnetic field intensity data over geological time periods are required to solve geoscience problems such as the dynamics of Earth's core, the thermal interaction of the

* Corresponding author.
E-mail address: taslima@ualberta.ca (T. Anwar).

http://dx.doi.org/10.1016/j.pepi.2016.09.007
0031-9201/

core-mantle boundary, the relationship between the mean paleointensity and the reversal frequency and the nucleation date of Earth's inner core (Glatzmaier et al., 1999; Tarduno et al., 2006; Christensen and Wicht, 2007; Biggin et al., 2012; Biggin et al., 2015). Although many studies have attempted to capture the detailed information about the variation in paleointensity, these are not sufficient enough to be reliable (see the absolute paleointensity PINT database; Biggin et al., 2010) due to the lack of proper materials and magnetomineralogical alterations during the experiments. Thus, it is important to get more reliable data about the history of Earth's magnetic field intensity to compare the behavior of geodynamo models with measured data on all accessible timescales.

Continental flood basalts (CFBs) are considered excellent objects for decoding the evolution of Earth's magnetic field since they are related to huge eruptions of lava flows during very short spans of volcanic activity. One of the largest CFBs is situated at and around the Siberian platform and was formed during the Permo-Triassic boundary (PTB) at approximately 250 Ma (Courtillot and Renne, 2003; Almukhamedov et al., 2004; Reichow et al., 2005, 2009, and references therein). This is a time interval when gigantic magma volumes erupted (Kuzmin et al., 2010), the largest mass extinction occurred, and dramatic climatic changes took place (Kravchinsky, 2012), and thus, this interval played a crucial role in Earth's geological history. This is also a period of particular interest concerning the characteristics of the dipolar field to investigate the extension of the Mesozoic dipole low (MDL), which is a time interval characterized by a dipole with a moment of approximately 30% of that of the present magnetic field (Prévot et al. 1990). The MDL hypothesis has also been supported by several other studies (Pick and Tauxe, 1993; Kosterov et al., 1998; Thomas and Biggin, 2003; Shcherbakova et al., 2011, 2012; Tauxe et al., 2013) although its duration is highly unclear.

Geomagnetic field directions are well known for the PTB, but paleointensity data are insufficient giving rise to a contradiction about the average dipole moment during this time period. Some studies from the northern part of the Siberian trap basalts (STB) have shown lower (approximately half) paleointensity values compared to the present day field and suggested that the MDL reached back to the PTB (Heunemann et al., 2004; Shcherbakova et al., 2005, 2013, 2015). By contrast, another study, conducted on the southeastern part of the STB, has indicated a possibility of higher absolute paleointensity values, almost equal to the present day field, and suggested that the MDL did not extend back to the PTB (Blanco et al., 2012). Previous studies used the conventional thermal Thellier-Thellier technique (Thellier and Thellier, 1959; Coe, 1967) to identify the ancient field intensity for the STB. However, the magnetic minerals in samples are sometimes chemically altered during thermal paleointensity experiments (Valet et al., 1996; Heller et al., 2002; Smirnov and Tarduno, 2003). Such studies were conducted on the sections of either the northern or the southeastern part of the formation. One argued source of discrepancy is that multi-domain behavior causing curvature of the Arai plots, with the lower paleointensity results coming from the high temperature components which are underestimates of the true paleointensity results. Another possibility is that this discrepancy is caused by secular variation and the geomagnetic field being recorded at slightly different times for the northern extrusive and southeastern intrusive localities, each being insufficiently large to provide a representative time average.

To derive whether Earth's magnetic field is weak or strong at that time period, further paleointensity measurements are required. Here, for the first time, this study presents the microwave paleointensity data of the PTB. The microwave paleointensity method (Walton et al., 1996; Hill and Shaw, 1999) minimizes the occurrence of magneto-mineralogical alteration which is the major problem associated with absolute paleointensity determination, resulting in a higher success rate compare to the conventional Thellier-Thellier method (Böhnel et al., 2003 and Biggin, 2010). Here, we intend to collate microwave Thellier-type paleointensity data of this study with the thermal Thellier-type paleointensity data of previous studies, and produce overall mean paleomagnetic dipole moment for the STB. This provides an opportunity to investigate the duration and characteristics of the MDL. Furthermore, Q_{PI} analyses (Biggin and Paterson, 2014; Biggin et al., 2015) performed on all the published data including this study for the Siberian Traps is presented. Moreover, this study covers a longer time interval involving both the extrusive and intrusive traps of the northern and the southeastern localities respectively, and thus, provides much wider geographical and spatial coverage.

2. Geological settings

The STB of the Siberian platform represents the largest terrestrial continental igneous province. ^{40}Ar–^{39}Ar radiometric dates indicate that Siberian trap volcanism was produced at the PTB (250 ± 1.6 Ma) (Renne et al., 1995; Reichow et al., 2002) and the geological evidence supports that these traps were deposited in a short time (0.9 ± 0.8 Ma) interval (Renne and Basu 1991) that did not exceed 2 Myr (Reichow et al., 2009). The enormous volcanic activity contributed the greatest mass extinction of flora and fauna in Earth's history (Courtillot and Renne, 2003). The emplacement of the Siberian Traps is coeval with a major environmental crisis (Erwin, 1994; Kravchinsky, 2012). These traps were built from one or more volcanic events involving the outpouring of large volumes of mainly basaltic magma. The volcanic sequence is about 6.5 km thick and the Permo-Triassic traps cover an area of approximately 3.7×10^6 km^2 with the original volume of almost 3.0×10^6 km^3 in the northern part of the Siberian platform and under the West Siberian sedimentary basin (Kravchinsky et al., 2002; Reichow et al., 2009; Kuzmin et al., 2010). The sills extend to the east and the southeast of the province with an approximate area of 1.5×10^6 km^2 (Zolotukhin and Al'mukhamedov, 1988). The magma source and emplacement mechanism of the traps can be described by numerous models. It is argued that the Siberian Traps were linked to the rifting triggered by an upwelling mantle plume (Basu et al., 1998; Griffin et al., 1999; Courtillot et al., 1999; Kuzmin et al., 2010) rather than volcanism at an existing plate boundary (Almukhamedov et al., 1996; Courtillot et al., 1999; Saunders et al., 2005; Kuzmin et al., 2010). It has been further argued that melt intrusions could have produced the Siberian Traps eruption (Elkins Tanton and Hager, 2000).

The Siberian Traps contain mafic, ultramafic, and silicic rocks, both intrusive and extrusive. In this study, samples from both the northern extrusive (Maymecha-Kotuy region) and the southeastern intrusive (Sytikanskaya and Yubileinaya kimberlite pipes) part of the Permo-Triassic trap basalts on the Siberian platform were analyzed (Fig. 1). Both these extrusive and intrusive localities are important to study as, together, these cover a longer time interval. Besides, these represent a huge territory providing a broad spatio-temporal representation of the PTB.

The Maymecha-Kotuy region, comprising ~70,000 km^2, is situated in the northern part of the Siberian platform and in the western Anabar region (location 1 on Fig. 1). The volcanic sequence is composed of the six formations, namely: Pravaboyar, Arydzhang, Onkuchak, Tyvankit, Delkan and Maymechin, overlying the Tunguss sedimentary series (Fig. 2). The total thickness of this volcanic sequence is 4 km (Fedorenko and Czamanske, 1997). Both the Pravaboyar Formation located in the lower part of the Maymecha section and the Arydzhang Formation situated in the lower part of the Kotuy section are dated at 251.7 ± 0.4 Ma, while the Delkan

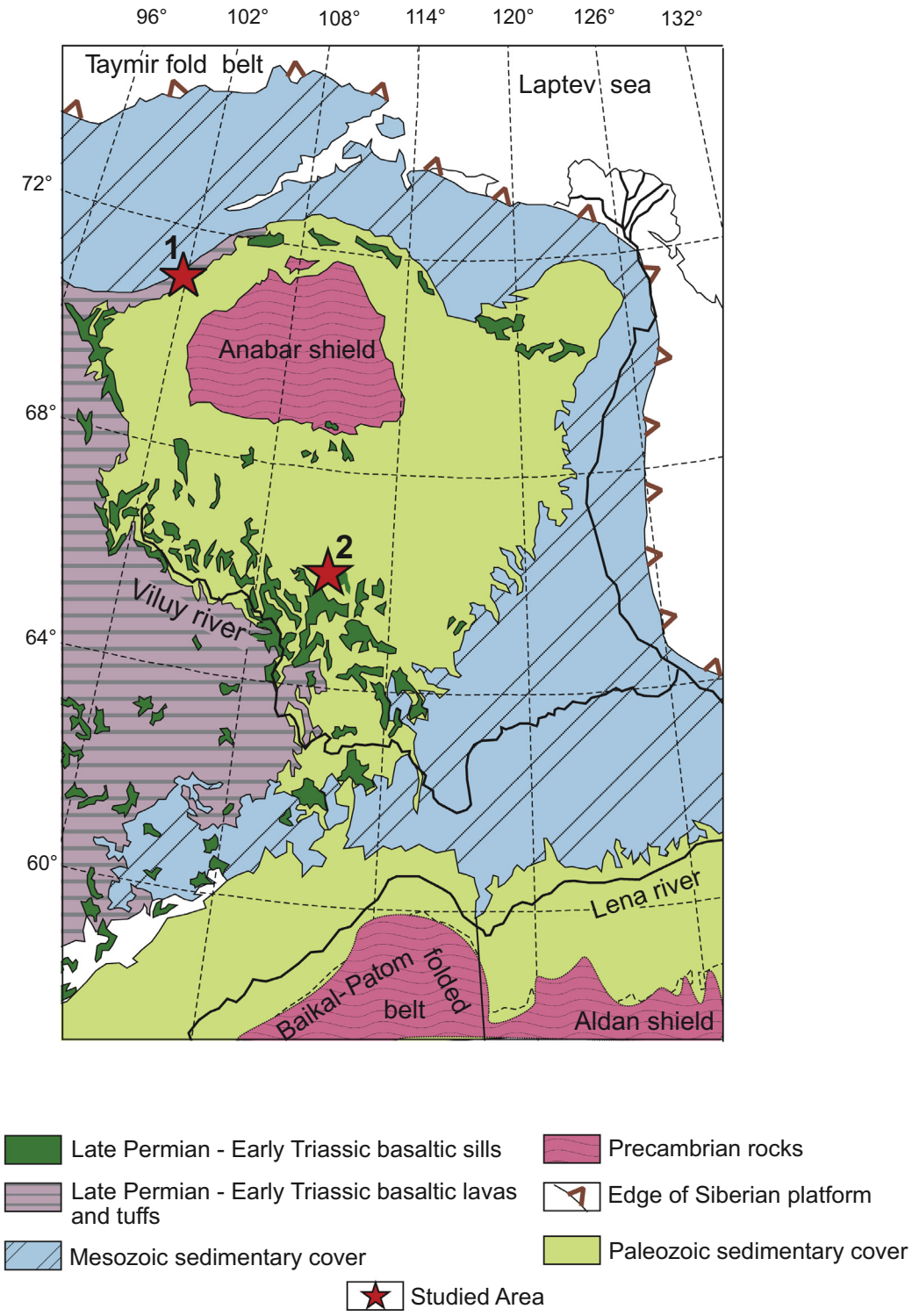

Fig. 1. Geological map of the Siberian Traps and the geographic positions of the studied sections (after Courtillot et al., 2010). Red stars represent the study areas: 1 – Maymecha-Kotuy region, 2 – East Siberian intrusives (Sytikanskaya and Yubileinaya pipes). (For interpretation of the references to colour in this figure legend, the reader is referred to the web version of this article.)

Formation, representing upper part of the volcanic sequence of the Maymecha region, is dated at 251.1 ± 0.3 Ma by absolute U-Pb dating of the perovskite (Kamo et al., 2003). More recent studies indicate ages for these formations correspondingly to be 252.24 ± 0.12 and 251.90 ± 0.061 Ma (Burgess and Bowring, 2015). We have studied the samples from the Truba section (T) (71.55° N, 103.00° E) which comprises of the Onkuchak Formation along the Kotuy river valley (10 km downstream from the Kayak village) and from the Maymecha section (M) (70.82° N, 101.00° E) which corresponds to the Tyvankit and Delkan Formations in the Maymecha river (opposite to the mouth of the Kogotok stream). While the Onkuchak Formation is mainly composed of the tholeiitic basalts, the studied intervals of the Tyvankit and Delkan Formations are represented essentially by trachybasalts and high-Ti meta-

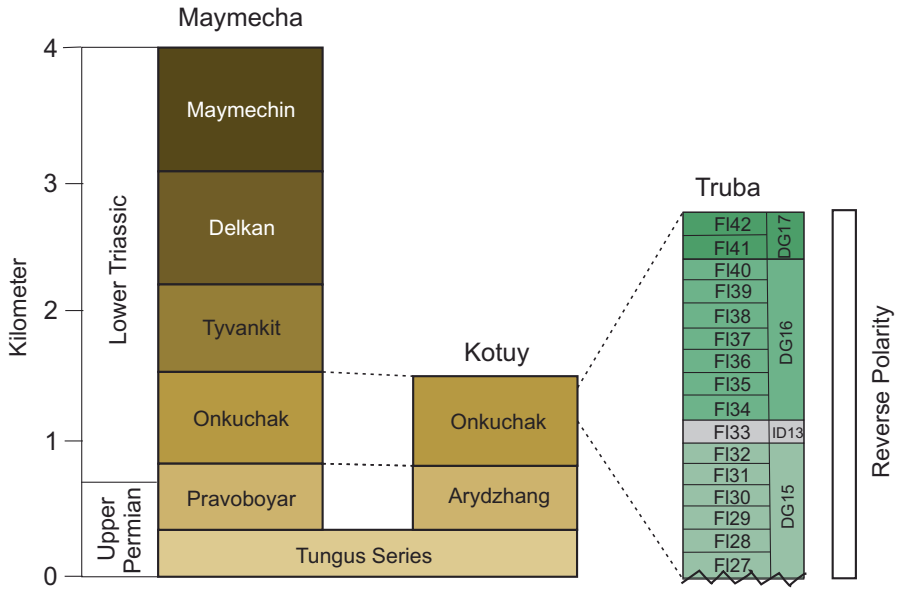

Fig. 2. The stratigraphy and correlation of the volcanic sequences of Maymecha and Kotuy regions. Fl; flow, DG; directional groups (pulses), ID; individual directions (individual eruptions). (Correlation scheme after Pavlov et al., 2015).

nephelenitic lavas correspondingly (Kamo et al., 2003). The Truba section at Kotuy contains 42 basaltic flows and the total thickness of these strata is about 360 m. Samples of the 4 flows (flow 28, flow 29, flow 35, and flow 40) from the Truba section of the Onkuchak Formation have been measured (Fig. 2). 17 directional groups (DG) and 13 individual directions (ID) were identified in the composite Kotuy section based on the analysis of the secular variations recorded in the lava flows, and the number of these DG and ID corresponds to the number of volcanic bursts and individual eruptions that formed the studied section (Pavlov et al., 2011, 2015). The division of the traps into separate lava flows was ambiguous for the Maymecha section; however, Shcherbakova et al. (2015) made an attempt to distinguish 42 lava flows and two intervals with undistinguishable flows (flows 1–34 are related to the Tyvankit Formation, and flows 35–42 are to the Delkan Formation) for this section. The total thickness of this section is about 380 m. Samples of the 3 flows (flow 23, flow 21, and flow 18) from the Maymecha section of the Tyvankit Formation have been measured. Paleomagnetic direction and magneto-mineralogical studies of these sections have already been published (Pavlov et al., 2011; Shcherbakova et al., 2013, 2015). Reversed polarity was identified for both the Truba section of the Onkuchak Formation (Fetisova et al., 2014; Pavlov et al., 2011), and the Maymecha section (Shcherbakova et al., 2015). Previous studies suggest that the main remanence carrier is titanomagnetite; for the Tyvankit Formation (Shcherbakova et al., 2015) and parts of the Onkuchak Formation (Shcherbakova et al., 2013), this is low titanium titanomagnetite with a Curie temperature close to pure magnetite, and for the rest of the Onkuchak Formation, the titanomagnetite is richer in titanium (Shcherbakova et al., 2013) with a depressed Curie temperature of 300–400 °C. The grains that carry the remanent magnetization for the studied rocks are single-domain or small pseudo-single domain (Pavlov et al., 2011; Shcherbakova et al., 2013, 2015).

A large part of the Siberian platform experienced only intrusive magmatism with extensive but relatively low-volume sills, which are hardly exposed on the surface and known mostly through drilling. For the southeastern part of the STB, 5–20 m thick intrusive (near surface intrusions) trap sills overlain in the area of Sytikanskaya (66.11° N, 111.80° E) and Yubileinaya (66.00° N, 111.70° E) kimberlite pipes have been studied (location 2 on Fig. 1). This is one of the most eastern occurrences of Permo-Triassic flood basalts on the Siberian platform. The intrusive bodies are considered to be trap-related and coeval with the flood basalts but the ages of these are difficult to measure directly (Zolotukhin and Al'mukhamedov, 1988). Usually, the smaller sills extend from the main sill intrusion and comprise a few square kilometers. We have studied the samples from three sites (S1, S2, S3) of the Sytikanskaya and one site (Y1) of the Yubileinaya kimberlite pipe. Although the exact time relationship between the sills is hard to establish, the samples of different sites may be related to few phases of eruption that should provide some representation of geomagnetic secular variation. Paleomagnetic directions from these sills have already been reported and show a stable component of remanent magnetization with the presence of antipodal polarities- normal polarity for the Yubileinaya and reverse polarity for the Sytikanskaya section (Kravchinsky et al., 2002 and Blanco et al., 2012). The rock magnetic studies indicate that the primary remanence carriers are composed of a low titanium titanomagnetite or pure magnetite, containing single or pseudo-single domain particles (Kravchinsky et al., 2002; Blanco et al., 2012; Konstantinov et al., 2014).

3. Methodology

3.1. Scanning Electron Microscope

Scanning Electron Microscope (SEM) analysis was performed on the carbon coated polished thin sections using a Zeiss EVO LS15 EP-SEM instrument equipped with energy dispersive X-ray (EDX) spectroscopy to identify the morphological features and the chemical composition of the magnetic minerals in the samples. The SEM is operated at an acceleration voltage of 20 kV. The SEM results are obtained in the Scanning Electron Microscope Laboratory of the University of Alberta (Edmonton, Canada).

3.2. Microwave paleointensity

In this study, absolute paleointensity has been investigated by using the internationally unique microwave paleointensity facility housed in the University of Liverpool's Geomagnetism Laboratory.

Table 1
Summary of the acceptance criteria for selecting paleointensity values of the individual samples.

Criterion	Threshold	Reference
Number of points (N)	$\geqslant 4$	
Scatter parameter (β)	$\leqslant 0.1$	Coe et al. (1978)
Fraction of the NRM (f)	$\geqslant 0.35$	Coe et al. (1978)
Quality factor (q)	$\geqslant 2$	Coe et al. (1978)
Difference ratio (DRAT)	$\leqslant 15\%$	Selkin and Tauxe (2000)
Maximum angle of deviation (MAD)	$\leqslant 15^\circ$	Kirschvink (1980)
Angular difference between anchored and floating PCA fit (α)	$\leqslant 15^\circ$	Selkin and Tauxe (2000)

For microwave paleointensity experiment, the high-frequency (14 GHz) microwaves are used instead of the conventional thermal energy to (de)magnetize the samples (Walton et al., 1996). The same experimental protocol can be used for both the microwave and thermal experiments (Hill and Shaw, 1999). In the thermal Thellier-Thellier method, phonons are responsible for the thermally induced alteration in samples. The microwave Thellier-Thellier technique minimizes the occurrence of magneto-mineralogical alteration by reducing the temperature that the bulk sample is heated to, and the duration of this heating (Hill and Shaw, 1999). This together with the fact that, unlike in batch heating experiments, measurement routines can be tailored to individual samples, tends to produce a higher success rate compared to the conventional Thellier-Thellier method (Böhnel et al., 2003; Biggin, 2010).

Microwave Thellier-type paleointensity experiments were performed using Liverpool's third generation system which incorporates three helium SQUID sensors, a triple-axis Helmholtz coil assembly surrounding the microwave resonant cavity, and vertical sample assembly with a vacuum holder. The samples were progressively demagnetized and remagnetized by the application of the high frequency (14 GHz) microwave radiation which was increased progressively in power and/or duration and the in-field/zero-field and zero-field/in-field (IZZI) protocol (Tauxe and Staudigel, 2004) was used for the paleointensity experiments. The experiment was usually continued until the NRM intensity was reduced to 10–20% of its original value. To test for sample alteration, partial thermoremanent magnetization (pTRM) checks (Coe, 1967 and Coe et al., 1978) were performed in all paleointensity experiments. Arai plots (Nagata et al., 1963) were used to analyze the results.

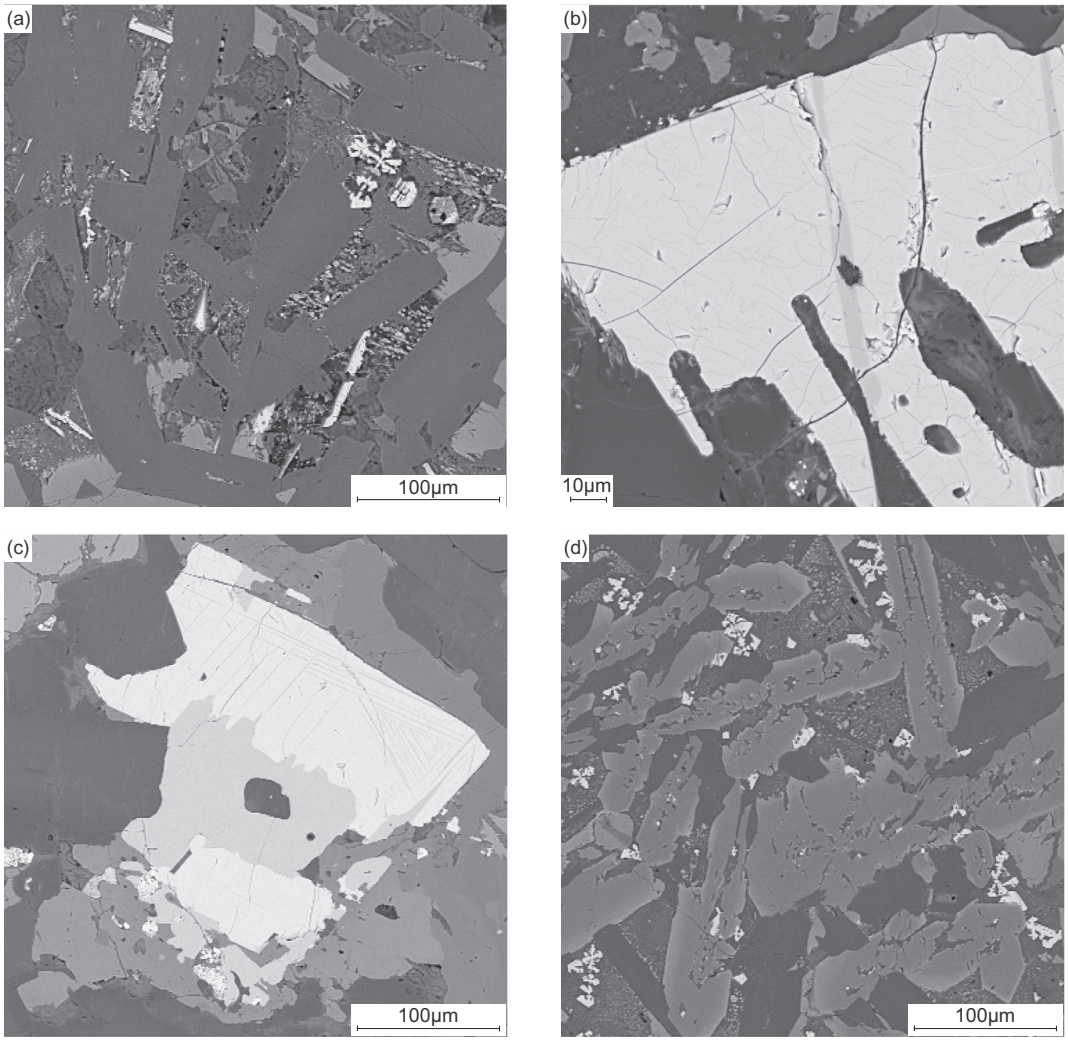

Fig. 3. Representative magnetic mineralogy of the samples that passed palaeointensity section criteria; (a) dendritic titanomagnetite and needles of ilmenite (sample 294; Truba, flow 28), (b) skeletal titanomagnetite with ilmenite lamellae (sample 304; Truba, flow 29), (c) subhedral magnetite grain (sample 15; Sytikanskaya pipe, site S1), and (d) dendritic titanomagnetite (sample 1; Yubileinaya pipe, site Y1).

In total, 50 samples (23 samples from the northern localities and 27 samples from the southeastern localities) from 11 sites [T (flow 28), T (flow 29), T (flow 35), T (flow 40), M (flow 23), M (flow 21), M (flow 18), S1, S2, S3, and Y1] of 4 areas (Truba, Maymecha, Sytikanskaya, and Yubileinaya) of the Permo-Triassic trap basalts on the Siberian platform were subjected to microwave Thellier-type paleointensity measurements. In the previous study, rock magnetic and paleomagnetic directional analysis of these samples for both the northern localities (Pavlov et al., 2011 and Shcherbakova et al., 2013, 2015) and the southeastern localities (Kravchinsky et al., 2002 and Blanco et al., 2012) showed that the remanent magnetization represents stable primary magnetization components and these samples are suitable for paleointensity determination. Samples of small size, typically 5 mm in diameter and 3–6 mm in length, have been used for the microwave technique. The laboratory field intensity applied to the samples ranges between 7 and 50 μT. The applied field value was changed for additional verification of the results, and these indicated that the absolute paleointensity values were independent of these values. Furthermore, the laboratory field applied at an angle of at least 45° to the NRM to ensure that multidomain-like behavior would manifest as zig-zags in both the Arai plot and the Zijderveld plot as the latter can be invisible if the applied field is (anti-)parallel to the NRM (Yu and Tauxe, 2005).

3.3. Paleointensity selection criteria

There are a number of parameters to describe the behavior of experimental paleointensity data (e.g., Coe et al., 1978; Kirschvink, 1980; Selkin and Tauxe, 2000; Tauxe and Staudigel, 2004; Biggin et al., 2007; Paterson, 2011; Yu, 2012). The parameters used in this study to produce the reliable absolute paleointensity data were calculated according to the Standardized Paleointensity Definitions (Paterson et al., 2014). The threshold values listed in Table 1 have been applied for the selection here. This includes- the number of data points used to estimate the paleointensity (N), standard error of the slope over the slope of the best fitting line (β), fraction of the total NRM that is chosen from NRM-TRM plot to recover the paleointensity estimate (f), the gap factor representing the evenness of point spacing along the selected best-fit-line (g), the quality factor which is the combination of several parameters (q), the pTRM difference ratio (DRAT) which is the absolute discrepancy between a pTRM check and an original measurement of pTRM divided by the length of the best-fit-line, the sum of all DRATs over the range of temperatures used for the paleointensity measurement (CDRAT), the maximum angular deviation (MAD) of the data points on a vector diagram determined from a free-floating fit without the origin included and the angle between the anchored and free floating best-fit directions on a vector component diagram (α).

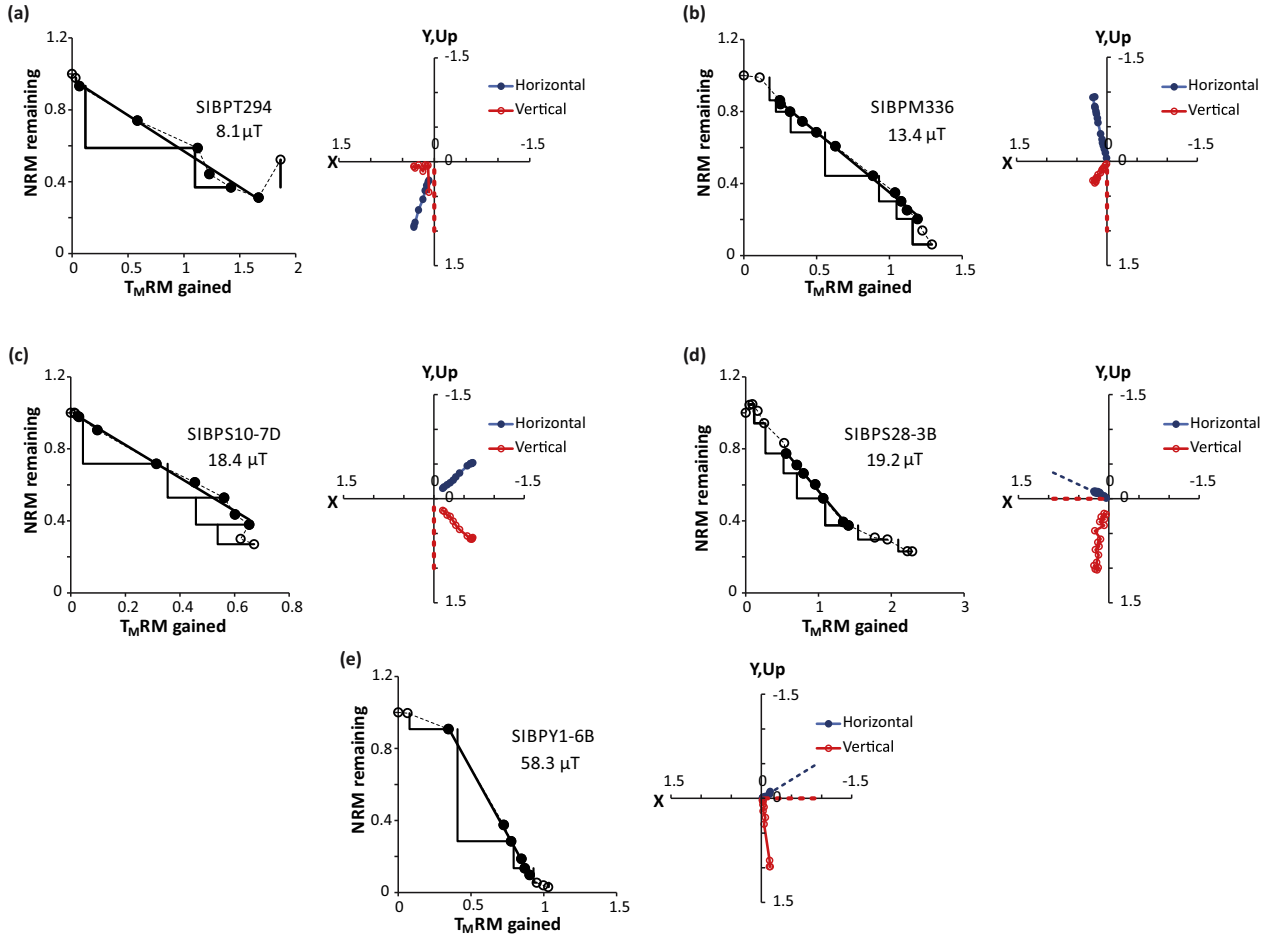

Fig. 4. Examples of Arai and associated Zijderveld plots produced by microwave Thellier method. Triangles on the Arai plots represent pTRM checks and the solid straight lines marks the interval on which intensity was estimated. On the Zijderveld plots, red (blue) points represent the vertical (horizontal) component (all samples were unoriented). (a) Truba (site T, flow 28) specimen, (b) Maymecha (site M, flow 23) specimen, (c) Sytikanskaya (site S1) specimen, (d) Sytikanskaya (site S3) specimen, and (e) Yubileinaya (site Y1) specimen. (For interpretation of the references to colour in this figure legend, the reader is referred to the web version of this article.)

4. Results and discussion

4.1. Scanning Electron Microscope

Six thin sections, one representing each site with accepted paleointensity results, were investigated using SEM analysis and compared to previously published petrographic and rock magnetic results. The magneto-mineralogy of the Truba section (flows 28 and 29) consists of titanomagnetite and ilmenite, as determined by Shcherbakova et al. (2013). The morphology of the magneto-mineral grains differs between the two flows, but both are consistent with rapidly cooling flows; T (flow 28) contains dendritic titanomagnetite and small needles of ilmenite (Fig. 3a), while T (flow 29) is dominated by large (>100 μm), skeletal titanomagnetite grains (Fig. 3b). A few lamellae are present suggesting that the titanomagnetite may have begun high-temperature, solid-state exsolution into magnetite and ilmenite. However, fast cooling of the flow may have prevented any significant exsolution occurring, resulting in the titanium rich titanomagnetite, confirmed by EDX analysis (the Ti:Fe ratio is ~37%). These samples most likely correspond to the low Curie temperature titanomagnetite (Tc ~300–400 °C). The EDX results also suggest that fractures in the large titanomagnetite grains of T (flow 29) experienced some secondary single-phase low-temperature oxidation but it is not clear whether this was sufficiently extensive to have had a substantial effect on the remanence. In comparison, the large (>100 μm), subhedral titanomagnetite grains in the Maymecha section (site M) represent a long cooling history that may account for the greater

Table 2
Microwave and previously published thermal Thellier paleointensity results during Permo-Triassic boundary. MW: Microwave paleointensity method, TT: Thellier-type paleointensity method and W: Wilson method (references: *[1]Shcherbakova et al., 2013, *[2]Shcherbakova et al., 2015 and *[3]Blanco et al., 2012). Hlab: applied laboratory magnetic field. N: number of successive data points used for paleointensity calculations. β, f, g and q are the measure of linearity, fraction of the NRM, the gap factor and the quality factor respectively. DRAT: percentage of discrepancy in the pTRM check. CDRAT: cumulative DRAT. MAD: maximum angular deviation. k': curvature of the Arai plot. PI: paleointensity result. VDM: Virtual dipole moment with its associated standard deviation. Samples that are in grey represent previously published results that have been rejected from our site means as the results do not appear to be reliable (see text for details). *[4]Indicates that quoted uncertainties are 95% confidence limits calculated according to Student's T distribution; in other cases, they are standard deviations.

Site	Sample	Method	Low Integral /Temp W.s / °C	High Integral /Temp W.s / °C	Hlab (μT)	N	β	f	g	q	delCK	DRAT	CDRAT	Alpha	MAD	k'	PI (μT)	Site Mean (μT)	VDM (x10[22] Am[2])
Truba																			
T (flow 28)	SIBPT294	MW	66	138	20	6	0.079	0.408	0.763	6.3	2.20%	3.10%	2.00%	4.3	3.4	-0.14	8.1		
	SIBPT294B	MW	95	362	10	13	0.045	0.369	0.856	6.4	4.80%	12.60%	12.00%	13	2.3	0.05	5.1		
	SIBPT294C	MW	63	141	7	7	0.033	0.609	0.664	13.3	6.50%	5.40%	8.80%	7.7	3.4	-0.14	10.6	7.9 ± 2.8	1.2 ± 0.4 (n=3)
	294(1)*[1]	TT	200	350	20	7	-	0.42	0.82	2.7	-	-	-	-	-		20.4		
	294(jr6)*[1]	TT	200	390	20	10	-	0.68	0.88	5.6	-	-	-	-	-		21.3		
	294(1)*[1]	W															14.3		
T (flow 29)	SIBPT304	MW	45	220	30	8	0.064	0.672	0.757	9.1	5.50%	6.50%	-7.90%	1.5	1.5	0.27	13.7		
	SIBPT307A	MW	80	216	15	9	0.021	0.593	0.865	29.6	12.20%	15.50%	32.40%	5.3	3		6.6		
	SIBPT307B	MW	65	167	10	7	0.101	0.36	0.799	3.8	1.50%	2.50%	-1.00%	6.2	1.9	0.49	7.9	9.4 ± 3.8	1.4 ± 0.6 (n=3)
	308(1)*[1]	TT	200	270	20	3	-	0.28	0.5	1	-	-	-	-	-		18.9		
	308(2)*[1]	TT	160	270	20	7	-	0.33	0.83	4	-	-	-	-	-		23.9		
	308(1)*[1]	W															23.6		
Maymecha																			
M (flow 23)	SIBPM336	MW	119	289	20	11	0.018	0.645	0.859	29.8	4.50%	5.90%	9.90%	2.4	1.6	-0.13	13.4		
	SIBPM336B	MW	135	293	20	9	0.036	0.584	0.85	13.5	5.20%	7.50%	-5.40%	5.5	6.1	-0.06	13.2		
	336*[2]	TT	500	620	20	13	-	0.58	0.89	35.2	-	-	-	-	-		10.8	11.0 ± 2.2	2.4 ± 0.5 (n=5)
	336_jr6*[2]	TT	450	580	20	12	-	0.58	0.88	10.3	-	-	-	-	-		8.7		
	336*[2]	W															9		
M (flow 21)	SIBPM346	MW	184	385	30	6	0.044	0.589	0.762	10.9	7.80%	9.80%	4.70%	0.3	1.5	-0.08	23.8	25.2 ± 2.0	5.4 ± 0.4 (n=2)
	SIBPM346B	MW	106	249	20	8	0.033	0.747	0.829	18.1	10.20%	8.50%	6.00%	1.3	0.8	-0.04	26.6		
Mean (northern sites)																		13.4 ± 12.7*[4]	2.6 ± 3.1*[4]
Sytikanskaya																			
S1	S8-9a*[3]	TT	450	575	30	5	0.1	0.95	0.49	3.8	-	-	-	-	-		18		
	SIBPS10-7B	MW	32	280	20	14	0.013	0.649	0.805	40.3	12.40%	14.50%	8.30%	7.6	2.6	-0.1	17.8		
	SIBPS10-7C	MW	102	166	20	6	0.102	0.604	0.591	4.2	11.10%	11.50%	8.50%	10.5	6	-0.37	17.5		
	SIBPS10-7D	MW	97	270	20	7	0.046	0.578	0.793	10	3.60%	4.60%	-6.30%	1.7	1.1	-0.18	18.4	18.6 ± 2.8	3.2 ± 0.5 (n=7)
	S15-1bf*[3]	TT	200	450	40	9	0.07	0.384	0.796	4.2	-	-	-	-	-		40.1		
	SIBPS15-6	MW	21	129	40	7	0.054	0.508	0.645	6.8	1.90%	2.90%	5.40%	3.5	1.1	0.32	21.2		
	SIBPS15-6B	MW	36	156	20	9	0.058	0.382	0.793	5.5	4.30%	6.90%	9.00%	4.1	1.1	0.35	23.1		
	SIBPS15-6C	MW	77	178	20	9	0.027	0.52	0.83	19.5	7.50%	9.80%	23.90%	6.3	4.2	0	14.3		
S3	SIBPS27-5	MW	93	336	40	12	0.048	0.778	0.859	11.8	10.10%	13.70%	-6.70%	7.7	7.5	-0.34	20.2		
	SIBPS27-5B	MW	123	191	20	4	0.083	0.375	0.625	3.3	4.30%	7.70%	11.70%	5.3	3.2	-0.47	15.2		
	S28-5b2*[3]	TT	350	575	25	7	0.07	0.86	0.77	9.1	-	-	-	-	-		28		
	SIBPS28-3B	MW	122	226	40	7	0.026	0.405	0.796	12	1.30%	2.90%	-5.70%	7.4	4.8	-0.05	19.2		
	SIBPS28-3C	MW	76	172	35	8	0.068	0.608	0.804	8.3	10.40%	13.50%	22.60%	8.3	4.4	0.19	15.3	16.0 ± 3.1	2.5 ± 0.5 (n=6)
	SIBPS28-3D	MW	69	153	20	7	0.086	0.349	0.769	3.4	3.90%	8.40%	9.80%	0.8	1	0.45	13.9		
	SIBPS30-11	MW	82	244	30	8	0.047	0.745	0.807	13.6	13.20%	15.30%	13.60%	2.2	5.6	-0.09	12.3		
	S32-4b*[3]	TT	375	475	40	5	0.1	0.32	0.72	1.4	-	-	-	-	-		40.78		
	S32-4bf*[3]	TT	375	500	40	6	0.1	0.49	0.79	2	-	-	-	-	-		49.28		
Mean (*Sytikanskaya*)																		17.3 ± 16.5*[4]	2.8 ± 4.4*[4]
Yubileinaya																			
Y1	Y51-3b*[3]	TT	250	550	80	7	0.02	0.87	0.76	24.4	-	-	-	-	-		36.25		
	Y52-3a*[3]	TT	300	525	40	10	0.1	0.89	0.77	4.4	-	-	-	-	-		44.9		
	Y52-4a*[3]	TT	250	525	35	7	0.04	0.82	0.76	15.3	-	-	-	-	-		44.7		
	SIBPY1-6B	MW	35	77	40	6	0.017	0.788	0.522	18	6.40%	6.30%	9.40%	1.8	2.3	-0.08	58.3		
	SIBPY1-6C	MW	39	80	50	5	0.054	0.589	0.628	5.7	8.50%	12.00%	22.20%	6.1	4.5	0.2	51.4	48.5 ± 7.3	6.4 ± 0.9 (n=8)
	SIBPY1-6D	MW	39	73	45	6	0.049	0.555	0.704	6.3	5.10%	7.30%	10.30%	6.1	4.4	-0.21	57.9		
	SIBPY4-2	MW	22	84	50	6	0.036	0.641	0.523	8.8	4.10%	5.20%	12.50%	8.1	7.7	-0.24	44.1		
	SIBPY4-2B	MW	30	60	50	4	0.093	0.429	0.579	2.8	4.20%	6.90%	9.00%	4.6	5.1	-0.43	47.5		
	SIBPY4-2C	MW	27	65	50	6	0.05	0.552	0.706	6.8	5.80%	8.70%	14.70%	5	4.2	-0.23	47.9		
Overall Mean																	N=7	19.5 ± 13.0*[4]	3.2 ± 1.8*[4]

number of lamellae from high-temperature, solid-phase exsolution than in the Truba section. The remainder of a small amount of high Ti titanomagnetite, that hadn't exsolved, is the probable cause of the small, non-reversible component in the Type A1 thermomagnetic curves from this section (Shcherbakova et al., 2015); however, all of the thermomagnetic curves gave a final Curie temperature close to that of magnetite.

For the Sytikanskaya kimberlite pipe (sites S1 and S3), EDX confirms that magnetite is present as a bimodal size distribution (Fig. 3c); as large, subhedral grains (50–300 μm long) and small magnetite grains (<10 μm), with neither containing any discernable titanium. The large grains also show that there is no fracturing to indicate the presence of secondary single-phase low-temperature oxidation. These grains are consistent with thermomagnetic curves for the Sytikanskaya pipe (Blanco et al., 2012), which are reversible and give a Curie temperature of ~560 °C, approximately that of pure magnetite. Comparatively, SEM analysis of Yubileinaya kimberlite pipe (site Y1) contains dendritic titanomagnetite and needle-like ilmenite crystals (Fig. 3d), similar to T (flow 28), although the proportion of titanomagnetite to ilmenite is much higher in the Yubileinaya sample. These results agree with the thermal dependent magnetic susceptibility curves that gave a Curie temperature of ~500 °C indicating the presence of a higher Ti content (Blanco et al., 2012).

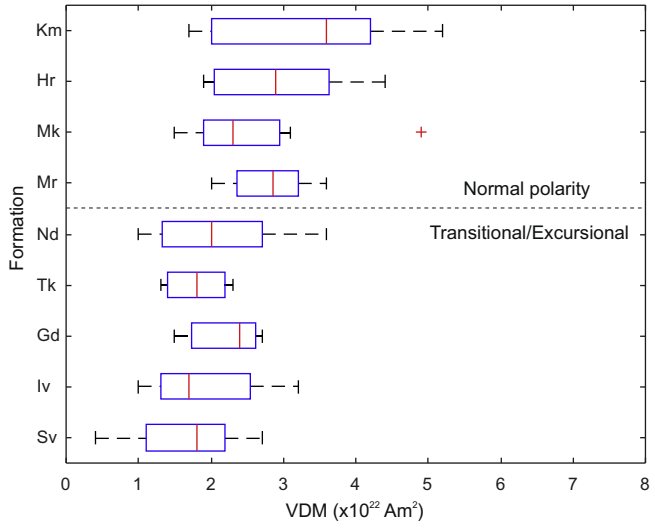

Fig. 5. The virtual dipole moment (VDM) results for Norilisk section sites listed in the PINT databse by Formation. km; Kumginsky Formation, Hr; Kharaelakhsky Formation, Mk; Mokulaevsky Formation, Mr; Morongovsky Formation, Nd; Nadezhdinsky Formation, Tk; Tuklonsky Formation, Gd; Gudchikhinsky Formation, Sv; Syverminskii Formation, Iv; Ivakinskii Formation. The Formations are listed in stratigraphic order (km is the youngest, Iv the oldest) but the axis is not scaled to time as the ages of the individual formations are unknown. The sections is considered to represent on the order of 10,000 years based on geomagnetic secular variation (Pavlov et al., 2015), with a change from an excursional and transitional field to normal polarity during Nd.

4.2. Microwave paleointensity

Fig. 4 presents examples of the accepted Arai plots along with the Zijderveld plots. Absolute microwave paleointensity results during the PTB with their associated quality factors are listed in Table 2. A total of 28 samples out of 50 samples from 7 sites of 4 areas satisfied the reliability criteria and were accepted. However, as only one sample from site M (flow 18) met the reliability criteria, this flow was not included in our result. No samples from site T (flow 35), T (flow 40) and S2 meet all the reliability criteria. The selected samples have shown corresponding distinct directional components, positive pTRM checks, no significant curvature of the Arai plots (k′ in Table 2; Paterson, 2011) and little or no zig-zagging of the Arai or Zijderveld plots (Fig. 4), supporting that the samples have not been influenced by lab-induced alteration or multi-domain behavior. In this study, the success rate for paleointensity determination is 56%.

The accepted microwave paleointensity results from this study are combined with some of the thermal Thellier-type and Wilson (Wilson, 1961) results from previously published studies (Table 2). For the Maymecha and Yubileinaya sites, the published thermal Thellier-type results are consistent with the new Microwave results. In contrast, there is a large degree of in-site dispersion when all of the results are combined for the Truba and Sytikanskaya sites, with site standard deviations of up to 55% of the site mean. Close analysis of the two accepted Truba flows reveals that the thermal paleointensity estimates are approximately double the value of the microwave results. One possible explanation for this discrepancy is that multidomain behavior was enhanced in one

Table 3
Q_{PI} (Quality of Paleointensity) summary for the Russian sites covering the Permo-Triassic boundary from the PINT database and this study. Medians and 95% uncertainties calculated using a bootstrp method are given.

Location	Qpi ⩾ 2	Qpi ⩾ 3	Qpi ⩾ 4	Qpi ⩾ 5	Qpi ⩾ 6
Northern Localities					
Maymecha-Kotuy					
No. of sites	41	41	41	24	6
VDM (×10^{22} Am^2)	2.2 + 0.2/−0.6	2.2 + 0.2/−0.6	2.2 + 0.2/−0.6	1.8 + 0.6/−0.3	2.40 + 0.7/−0.8
Norilisk					
No. of sites	52	49	33	0	0
VDM (×10^{22} Am^2)	3.1 ± 0.3	3.1 ± 0.3	2.8 + 0.4/−0.6	–	–
Total Northern Localities					
No. of sites	93	90	74	24	6
VDM (×10^{22} Am^2)	2.5 + 0.5/−0.2	2.5 + 0.4/−0.2	2.3 + 0.2/−0.1	1.8 + 0.6/−0.3	2.4 + 0.7/−0.8
Eastern Localities					
Aikhal, Sytikanskaya and Yubileinaya					
No. of sites	9	7	3	2	2
VDM (×10^{22} Am^2)	6.3 + 0.2/−3.1	6.3 + 0.1/−3.1	3.2	4.8	4.8
Siberian Traps Mean					
All sites					
No. of sites	102	97	77	26	8
VDM (×10^{22} Am^2)	2.8 ± 0.4	2.6 + 0.4/−0.3	2.3 + 0.3/−0.1	2.0 ± 0.5	2.6 + 0.8/−0.7

set of experiments over the other. In particular, we note that in the thermal Thellier experiments performed by Shcherbakova et al. (2013), no checks for MD behavior were performed and fraction (f) values from three out of the four estimates were less than 0.5. The use of the IZZI protocol in the microwave experiments and the resulting increased quality (q) values leads us to favour the new results over the old ones and thereby exclude the significantly higher thermal estimates from these two site means (Table 2; greyed out results). For the Sytikanskaya kimberlite pipe (sites S1 and S3), some of the thermal results are consistent with the microwave results while others are approximately twice as high. Blanco et al. (2012) divided the accepted thermal paleointensity results in two categories- 'A' and 'B'; the 'A' category results met all the reliability criteria defined by Selkin and Tauxe, (2000) whereas the results fell into the 'B' category if one of the reliability criteria failed one of these but otherwise fell into the following limits: 10% < meanDEV < 25%, 20% < pTRM tail check <25% and 30% < f < 60%. Since the 'B' category results are more prone to biasing from either laboratory induced alteration and/or MD effects, we exclude them from the site means for the Sytikanskaya (sites S1 and S3) and the Yubileinaya (site Y1) kimberlite pipe (Table 2; greyed out results).

The mean geomagnetic field intensity obtained from the four northern extrusive sites [T (flow 28), T (flow 29), M (flow 23), and M (flow 21)] is 13.4 ± 12.7 μT (95% confidence limits calculated using the Student's T distribution). This is slightly lower than the Sytikanskaya mean (17.3 ± 16.5 μT, sites S1 and S3) and substantially lower than the Yubileinaya (Y1) site mean (48.5 ± 7.3 μT). Furthermore, a nonparametric Mann-Whitney U Test, based on the individual specimen estimates rejects the null hypothesis of equality of medians between any two of the three regions at the 99% significance level.

A similar regional discrepancy has been pointed out earlier by Blanco et al. (2012) and was suggested to be a consequence of bias from multidomain behavior in northern specimens (resulting from reductions of the paleointensity estimates made from at high temperatures portions of the Arai plots). The present study does not support this explanation as the discrepancy remains even within a result set that showed little evidence of zigzagging and generally lower curvature parameters (k' in Table 2; Paterson, 2011).

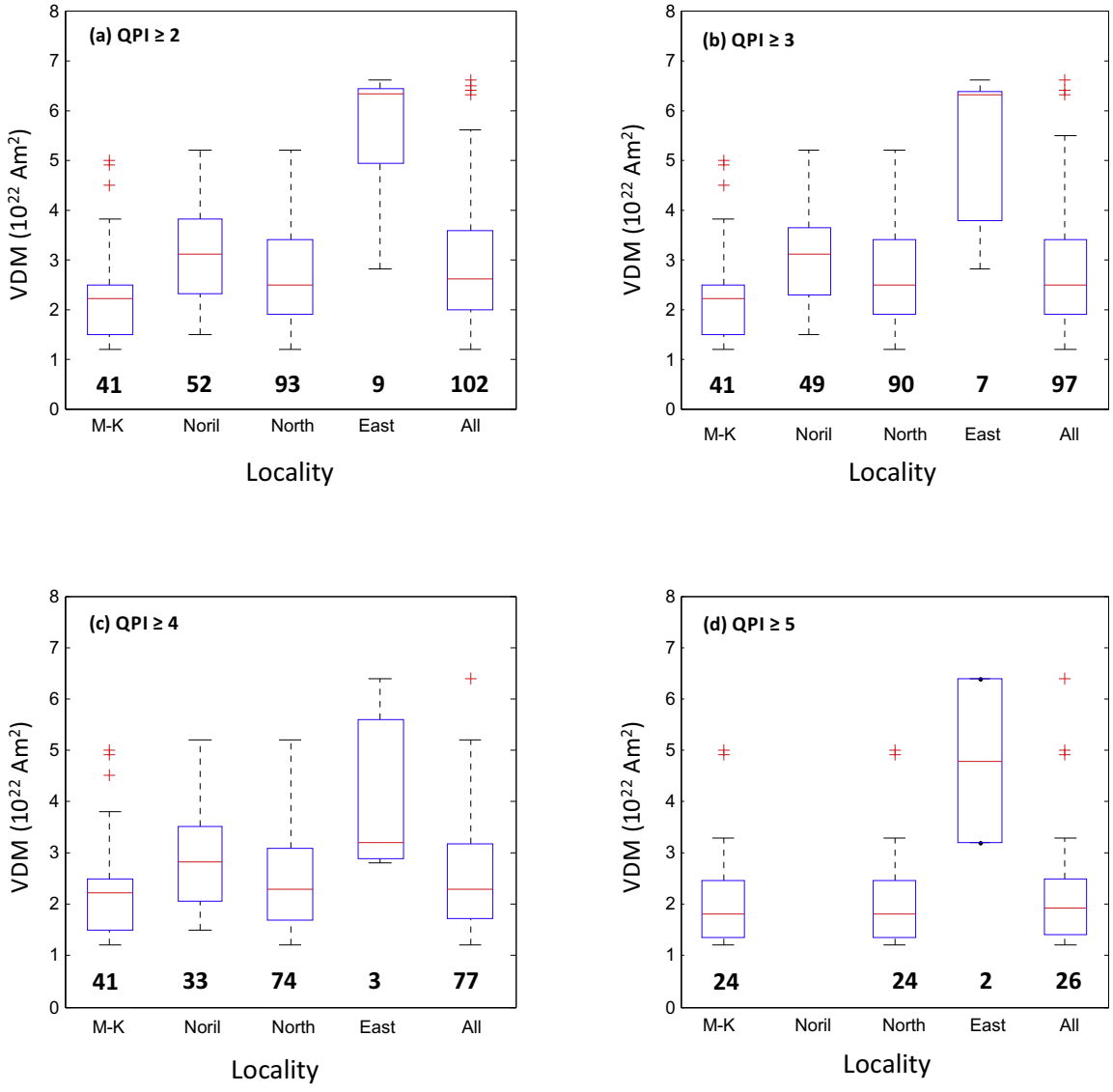

Fig. 6. The virtual dipole moment (VDM) results from the PINT database and this study, by location, filtered for their Q_{PI} values. (a) sites with Q_{PI} values $\geqslant 2$, (b) sites with Q_{PI} values $\geqslant 3$, (c) sites with Q_{PI} values $\geqslant 4$ and (d) sites with values $Q_{PI} \geqslant 5$. M-K; Maymecha-Kotuy, Noril; Norilisk, North; Northern Localities of Maymecha-Kotuy and Norilisk, East; Eastern Localities of Aikhal, Sytikanskaya and Yubileinaya, and All; All of the PTB Siberia sites from the PINT database and this study. The number of sites represented by each boxplot is shown below the boxes.

Another possibile cause that we rule out is crustal magnetic anomalies as these are weak in the region considered (Abramova and Abramova, 2014).

Our preferred explanation is simply that the regional discrepancy reflects slightly different time intervals within the 0.1–2 Myr emplacement event. Pavlov et al. (2015) estimates that the formation of the Norilisk and Maymecha-Kotuy sections "did not exceed a time interval on the order of 10,000 years" based on secular variation analysis of the directions from the Truba section and the Norilisk section (directions from Heunemann et al., 2004). Therefore, in the context of rates of secular variation such as that seen in the last 2 Myr (Valet et al., 2005), it is perfectly feasible that the units from the northern, Sytikanskaya and Yubileinaya sites were emplaced during time periods perhaps a few tens or hundreds of kyr apart when the field was in a different intensity regime.

It is also worth noting that Pavlov et al. (2015) suggests that thick parts of the sequence towards the base of the Norilisk section: the upper part of the Ivakinskii Formation to the lower part of the Nadezhdinsky Formation, represent those of a transitional and/or excursional field. The published paleointensity results from these formations seem to be in agreement with this analysis as the VDM results are consistently lower than those form the same section in a distinct polarity zone (Fig. 5). None of the samples from this transitional part of the section have been used for microwave analysis and we exclude these published results from our composite analysis outlined in the next section.

In this study, the overall mean paleointensity calculated using all seven site means is 19.5 ± 13.0 μT which corresponds to a mean virtual dipole moment (VDM) of $3.2 \pm 1.8 \times 10^{22}$ Am^2. Our results therefore support that the average magnetic field intensity during these short intervals is significantly lower (approximately half) than the present geomagnetic field intensity.

4.3. Collation of published data and Q_{PI} (Quality of Paleointensity) analysis

There are currently five published paleointensity studies for the Permo-Triassic Siberian Traps listed in the PINT database (Biggin et al., 2010), that have not been superseded by another publication. All of the sites listed in these publications, along with the sites in this study and that of Shcherbakova et al., 2015 (which have also not yet been added to the database), have been collated and assessed. Each site mean VDM value was assigned a Q_{PI} value based on the number of criteria (Biggin and Paterson, 2014) that the estimate passed. Supplementary Table provides the directions, intensities, and the complete breakdown of the estimation of Q_{PI} values for all the published studies along with this one. The sites cover three regions- the two northern regions (Maymecha-Kotuy and Norilsk) which have distinct but correlatable stratigraphy, and the southeastern region which contains the sills from the areas around the kimberlite pipes Sytikanskaya, Yubileinaya and Aikhal. To test the robustness of the geomagnetic means from these regions, sites were filtered out based on their Q_{PI} values to see how the site mean changed as less reliable sites were removed (Table 3 and Fig. 6).

For the northern localities, both of the regions have similar median paleointensities and show minimal variation with Q_{PI} filtering, as shown in Fig. 6. For up to $Q_{PI} \geqslant 5$, the Norilsk section has a much greater range due to the larger number of sites associated with this locality. There is a much greater variation in the median with Q_{PI} filtering for the southeastern localities because there are very few sites but the geomagnetic mean always remains significantly higher than the northern localities. The northern sites represent ~ 90% of the total sites studied indicating that the overall median is likely to be heavily biased by the potentially short-lived and extreme secular variation represented by the northern sites. Nevertheless, we point out that the simple average of the median northern and eastern regional results would still yield a dipole moment of only approximately half the present-day value.

4.4. Comparison to the Phanaerozoic record

Dipole moments based on different rock types for Permian to Cretaceous (300–65 Ma) are shown in Fig. 7 to allow investigation of the extent of the MDL behavior. Here, the paleointensity data of previously published 55 different studies, archived in the 2015 ver-

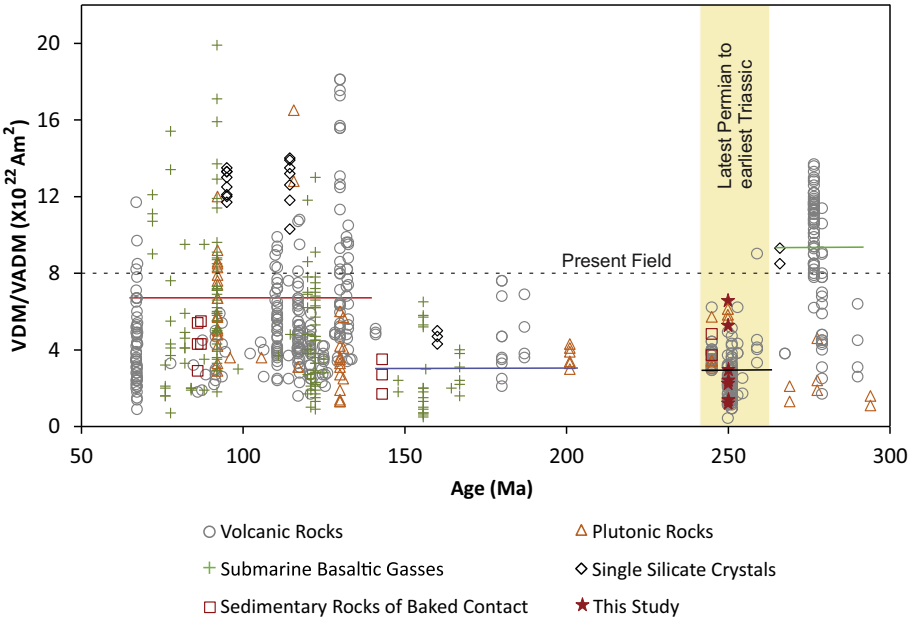

Fig. 7. The virtual dipole moment (VDM) and virtual axial dipole moment (VADM) from Permian to Cretaceous (300–65 Ma), obtained from the PINT database and the data from this study. The dashed horizontal line represents the strength of the present geomagnetic dipole moment. Solid horizontal lines represent the average geomagnetic dipole moment for Permian (green), Permo-Triassic boundary (black), Jurassic (blue) and Cretaceous (red). (For interpretation of the references to colour in this figure legend, the reader is referred to the web version of this article.)

sion of the PINT database (http://earth.liv.ac.uk/pint/), and this study are analyzed. As geomagnetic field intensities vary across geographic locations, the VDM or VADM record is used for this analysis. It is obvious that there is a degree of variability of dipole moment between different materials, such as volcanic rock, submarine basaltic glasses, plutonic rocks etc. Geomagnetic field strength recorded in submarine basaltic glasses, plutonic rocks and single silicate crystals is high relative to volcanic rocks and baked sedimentary rocks (Chang et al., 2013). The mean VDM/VADM of entire rock types for Permian (9.3×10^{22} Am^2) is higher than that of present day (8×10^{22} Am^2), whereas it is lower for the other three time intervals – PTB (2.7×10^{22} Am^2 for the PINT database and 3.2×10^{22} Am^2 for this study), Jurassic (3.3×10^{22} Am^2) and Cretaceous (6.7×10^{22} Am^2) (Fig. 7). The mean VDM/VADM has changed during the last 300 Ma indicating a period of low dipole moment during the Mesozoic, at least for the Jurassic (140–200 Ma), and, not withstanding a ~50 Myr gap in the record during the Triassic, now might extend to the PTB.

5. Conclusions

(1) Microwave paleointensity results for the PTB considering both the northern extrusive and the southeastern intrusive parts of the Siberian trap basalt are reported for the first time in this study.
(2) The results indicate that the average geomagnetic intensity for the different regions are distinctly different (being especially low – 13.4 ± 12.7 μT – in the northern extrusive localities and especially high – 48.5 ± 7.3 μT – in the single site from the Yubileinaya intrusives). This most likely reflects slightly different sampling of secular variation by the different suites of rocks. It demonstrates that it is important to consider multiple localities to evaluate the mean paleointensity for the PTB.
(3) In this study, the mean paleointensity recorded by the seven sites of the STB is 19.5 ± 13.0 μT which produces an overall mean virtual dipole moment (VDM) of $3.2 \pm 1.8 \times 10^{22}$ Am^2. This is higher than the mean paleointensity (2.7×10^{22} Am^2) from the PINT database, but this is due to a bias towards the number of sites in the northern regions, which is less of a problem in this study. These results are considered to be reliable and have Q_{PI} values $\geqslant 4$.
(4) Results demonstrate that published northern localities show minimal variation with Q_{PI} filtering, whereas Eastern localities show much greater variation as there are very few studied sites. Therefore, further work is required to improve the number of sites in the eastern localities, and this will help to determine a more representative value for the strength of the field at the PTB.
(5) Results suggest that the magnetic field intensity during this period was significantly lower (approximately half) than the present geomagnetic field intensity, and, could indicate that the MDL began at the PTB. New paleointensity data from Triassic age rocks are urgently required to test this hypothesis.

Acknowledgements

We thank Elliot Hurst (Geomagnetism Laboratory, University of Liverpool) and Gerein Nathan (Scanning Electron Microscope Lab, University of Alberta) for their assistance during the laboratory measurements. We express our gratitude to Anton Latyshev for providing the information on the Maymecha section. This study was partially funded by the Royal Society for A.J.B and V.A.K. The SEM measurements were performed using V.A.K.'s funds from Natural Sciences and Engineering Research Council of Canada (NSERC). V.E.P. was supported by the Grants 15-55-10055, 16-05-04446 from the Russian Foundation of Basic Research and Grant 14. Z50.31.0017 of the Government of the Russian Federation. The field trips were funded by ALROSA and Russian Academy of Sciences. We would also like to thank the reviewers, Greig A. Paterson and Jean-Pierre Valet, for their valuable comments and suggestions which significantly improved this manuscript.

Appendix A. Supplementary data

Supplementary data associated with this article can be found, in the online version, at http://dx.doi.org/10.1016/j.pepi.2016.09.007.

References

Abramova, D.Y., Abramova, L.M., 2014. Lithospheric magnetic anomalies in the territory of Siberia (from measurements by the CHAMP satellite). Russ. Geol. Geophys. 55 (7), 854–863.
Almukhamedov, A.I., Medvedev, A.Ya., Mitchell, C., Zolotukhin, V.V., 1996. Flood basalts in the core of the Tunguska syneclinse: comparative geochemistry. Russ. Geol. Geophys. Novosibirsk 37, 3–16 (in Russian).
Almukhamedov, A.I., Medvedev, A.Ya., Zolotukhin, V.V., 2004. Compositional evolution of the Permian-Triassic basalts of the Siberian Platform in time and space. Petrology 2 (4), 339–353 (in Russian).
Basu, A.R., Hannigan, R.E., Jacobsen, S.B., 1998. Melting of the Siberian mantle plume. Geophys. Res. Lett. 25, 2209–2212.
Biggin, A.J., 2010. Are systematic differences between thermal and microwave Thellier-type palaeointensity estimates a consequence of multidomain bias in the thermal results? Phys. Earth Planet. Inter. 180, 16–40.
Biggin, A.J., Paterson, G.A., 2014. A new set of qualitative reliability criteria to aid inferences on palaeomagnetic dipole moment variations through geological time. Front. Earth Sci. 2 (24), 1–9.
Biggin, A.J., Perrin, M., Dekkers, M.J., 2007. A reliable absolute palaeointensity determination obtained from a non-ideal recorder. Earth Planet. Sci. Lett. 257, 545–563.
Biggin, A.J., McCormack, A., Roberts, A., 2010. Paleointensity database updated and upgraded. Eos Trans. AGU 91 (2), 15.
Biggin, A.J., Steinberger, B., Aubert, J., Suttie, N., Holme, R., Torsvik, T.H., Van der Meer, D.G., Van Hinsbergen, D.J.J., 2012. Possible links between long term geomagnetic variations and whole-mantle convection processes. Nat. Geosci. 8, 526–533.
Biggin, A.J., Piispa, E., Pesonen, L.J., Holme, R., Paterson, G.A., Veikkolainen, T., Tauxe, L., 2015. Palaeomagnetic field strength variations suggest Mesoproterozoic inner core nucleation. Nature 525, 245–248.
Blanco, D., Kravchinsky, V.A., Valet, J.P., Ali, A., Potter, D.K., 2012. Does the Permo-Triassic geomagnetic dipole low exist? Phys. Earth Planet. Inter. 204–205, 11–21.
Böhnel, H., Biggin, A.J., Walton, D., Shaw, J., Share, J.A., 2003. Microwave palaeointensities from a recent Mexican lava flow, baked sediments and reheated pottery. Earth Planet. Sci. Lett. 214 (1–2), 221–236.
Burgess, S.D., Bowring, S.A., 2015. High-precision geochronology confirms voluminous magmatism before, during, and after Earth's most severe extinction. Sci. Adv. 1 (7), e1500470.
Coe, R.S., 1967. Palaeointensities of the Earth's magnetic field determined from tertiary and quaternary rocks. J. Geophys. Res. 72, 3247–3262.
Coe, R.S., Grommé, C.S., Mankinen, E.A., 1978. Geomagnetic paleointensities from radiocarbon dated lava flows on Hawaii and the question of the Pacific nondipole low. J. Geophys. Res. 83, 1740–1756.
Courtillot, V., Renne, P.R., 2003. On the ages of flood basalt events. C.R. Geosci. 335, 113–140.
Courtillot, V., Jaupart, C., Manighetti, I., Tapponnier, P., Besse, J., 1999. On causal links between flood basalts and continental breakup. Earth Planet. Sci. Lett. 166, 177–195.
Courtillot, V., Kravchinsky, V.A., Quidelleur, X., Renne, P.R., Gladkochub, D.P., 2010. Preliminary dating of the Viluy traps (Eastern Siberia): Eruption at the time of Late Devonian extinction events? Earth Planet. Sci. Lett. 300, 239–245.
Chang, B., Kim, W., Doh, S.J., Yu, Y., 2013. Paleointensity determination of Late Cretaceous basalts in northwest South Korea: implications for low and stable paleofield strength in the Late Cretaceous. Earth Planets Space 65, 1501–1513.
Christensen, U.R., Wicht, J., 2007. Numerical dynamo simulations. Treatise Geophys. 8, 245–282.
Elkins Tanton, L.T., Hager, B.H., 2000. Melt intrusion as a trigger for lithospheric foundering and the eruption of the Siberian flood basalts. Geophys. Res. Lett. 27, 3937–3940.
Erwin, D.H., 1994. The Permo-Triassic extinction. Nature 367, 231–236.
Fedorenko, V., Czamanske, G., 1997. Results of new field and geochemical studies of the volcanic and intrusive rocks of the Maymecha-Kotuy Area, Siberian Flood-Basalt Province. Int. Geol. Rev. 39, 479–531.
Fetisova, A.M., Veselovskii, R.V., Latyshev, A.V., Rad'ko, V.A., Pavlov, V.E., 2014. Magnetic stratigraphy of the Permian-Triassic traps in the Kotui River valley

(Siberian Platform): new paleomagnetic data. Stratigr. Geol. Correl. 22 (4), 377–390.
Glatzmaier, G.A., Coe, R.S., Hongre, L., Roberts, P.H., 1999. The role of the Earth's mantle in controlling the frequency of geomagnetic reversals. Nature 401, 885–890.
Griffin, W.L., Ryan, C.G., Kaminsky, F.V., O'Reilly, S.Y., Natapov, L.M., Win, T.T., Kinny, P.D., Ilupin, I.P., 1999. The Siberian lithosphere traverse, mantle terranes and the assembly of the Siberian Craton. Tectonophysics 310, 1–35.
Heller, R., Merrill, R.T., McFadden, P.L., 2002. The variation of intensity of earth's magnetic field with time. Phys. Earth Planet. Inter. 131 (3–4), 237–249.
Heunemann, C., Krasa, D., Soffel, H.C., Gurevitch, E., Bachtadse, V., 2004. Directions and intensities of the Earth's magnetic field during a reversal: results from the Permo-Triassic Siberian trap basalts. Russia. Earth Planet. Sci. Lett. 218, 197–213.
Hill, M.J., Shaw, J., 1999. Palaeointensity results for historic lavas from Mt Etna using microwave demagnetization/remagnetization in a modified Thellier-type experiment. Geophys. J. Int. 139 (2), 583–590.
Kamo, S.L., Czamanske, G.K., Amelin, Y., Fedorenko, V.A., Davis, D.W., Trofimov, V.R., 2003. Rapid eruption of siberian flood_volcanic rocks and evidence for coincidence with the Permian-Triassic boundary and mass extinction at 251 Ma. Earth Planet. Sci. Lett. 214, 75–91.
Kirschvink, J.L., 1980. The least-squares line and plane and the analysis of palaeomagnetic data. Geophys. J. R. Astron. Soc. 62 (3), 699–718.
Konstantinov, K.M., Bazhenov, M.L., Fetisova, A.M., Khutorskoy, M.D., 2014. Paleomagnetism of trap intrusions, East Siberia: Implications to flood basalt emplacement and the Permo-Triassic crisis of biosphere. Earth Planet. Sci. Lett. 394, 242–253.
Kosterov, A.A., Perrin, M., Glen, J.M., Coe, R.S., 1998. Paleointensity of the Earth's magnetic field in Early Cretaceous time: the Paraná Basalt. Brazil. J. Geophys. Res. 103, 9739–9753.
Kravchinsky, V.A., 2012. Paleozoic large igneous provinces of Northern Eurasia: correlation with mass extinction events. Global Planet. Change 86–87, 31–36.
Kravchinsky, V.A., Konstantinov, K.M., Courtillot, V., Savrasov, J.I., Valet, J.P., Cherniy, S.D., Mishenin, S.G., Parasotka, S., 2002. Palaeomagnetism of the east Siberian traps and kimberlites: two new poles and palaeogeographic reconstruction at about 360 and 250 Ma. Geophys. J. Int. 148, 1–33.
Kuzmin, M.I., Yarmolyuk, V.V., Kravchinsky, V.A., 2010. Phanerozoic hot spot traces and paleogeographic reconstruction of the Siberian continent based on interaction with the African large low shear velocity province. Earth Sci. Rev. 102, 29–59.
Nagata, T., Arai, Y., Momose, K., 1963. Secular variation of the geomagnetic total force during the last 5000 years. J. Geophys. Res. 68, 5277–5281.
Paterson, G.A., 2011. A simple test for the presence of multidomain behavior during paleointensity experiments. J. Geophys. Res. (Solid Earth) 116, B10104.
Paterson, G.A., Tauxe, L., Biggin, A.J., Shaar, R., Jonestrask, L.C., 2014. On improving the selection of paleointensity data. Geochem. Geophys. Geosyst. 15, 1180–1192.
Pavlov, V.E., Fluto, F., Veselovskii, R.V., Fetisova, A.M., Latyshev, A.V., 2011. Secular geomagnetic variations and volcanic pulses in the Permian-Triassic traps of the Norilsk and Maymecha-Kotui Provinces. Maymecha Izv. Phys. Solid Earth 47 (5), 402–417.
Pavlov, V., Fluteau, F., Veselovskiy, R., Fetisov, A., Latyshev, A., Elkins-Tanton, L.T., Sobolev, A., Krivolutskaya, N., 2015. Volcanic pulses in the siberian traps as inferred from Permo-Triassic geomagnetic secular variations. In: Schmidt, A., Fristad, K., Elkins-Tanton, L. (Eds.), Volcanism and Global Environmental Change. Cambridge University Press, United Kingdom, pp. 63–78.
Pick, T., Tauxe, L., 1993. Geomagnetic palaeointensities during the Cretaceous normal superchron measured using submarine basaltic glass. Nature 366, 238–242.
Prévot, M., El_Messaoud Derde, M., McWilliams, M., Thompson, J., 1990. Intensity of the Earth's magnetic field: evidence for a Mesozoic dipole low. Earth Planet. Sci. Lett. 97, 129–139.
Reichow, M.K., Saunders, A.D., White, R.V., Pringle, M.S., Mukhamedov, A.I., Medvedev, A.I., Kirda, N.P., 2002. Ar-40/Ar-39 dates from the West Siberian Basin: Siberian flood basalt province doubled. Science 296, 1846–1849.
Reichow, M.K., Saunders, A.D., White, R.V., Almukhamedov, A.I., Medvedev, A.Ya., 2005. Geochemistry and petrogenesis of basalts from the West Siberian Basin: an extension of Permo-Triassic Siberian Traps, Russia. Lithos 79, 425–452.
Reichow, M.K., Pringle, M.S., Al'Mukhamedov, A.I., Allen, M.B., Andreichev, V.L., Buslov, M.M., Davies, C.E., Fedoseer, G.S., Fitton, J.G., Inger, S., Medvedev, A.Ya., Mitchell, Puchkov, V.N., Safonava, I.Yu., Scoot, R.A., Saunders, A.D., 2009. The timing and the extent of the eruption of the Siberian traps large igneous province. Implications for the end-Permian environmental crisis. Earth Planet. Sci. Lett. 227, 9–20.
Renne, P.R., Basu, A.R., 1991. Rapid eruption of the Siberian Traps Flood Basalts at the Permo-Triassic boundary. Science 253, 176–179.
Renne, P.R., Zhang, Z.C., Richards, M.A., Black, M.T., Basu, A.R., 1995. Synchrony and causal relations between Permian-Triassic boundary crises and Siberian flood volcanism. Science 269, 1413–1416.
Saunders, A.D., Englend, R.W., Reichow, M.K., White, R.W., 2005. A mantle plume origin for the Siberian traps: uplift and extension in the West Siberian Basin, Russia. Lithos 79, 407–424.
Selkin, P.A., Tauxe, L., 2000. Long-term variations in palaeointensity. Philos. Trans. R. Soc. Lond. A 358 (1768), 1065–1088.
Shcherbakova, V.V., Shcherbakov, V.P., Vodovozov, V.V., Sycheva, N.K., 2005. Paleointensity at the Permian_Triassic boundary and in the late Permian. Izv. Acad. Sci. Phys. Solid Earth 41 (11), 931–944.
Shcherbakova, V.V., Kovalenko, D.V., Shcherbakov, V.P., Zhidkov, G.V., 2011. Paleointensity of the geomagnetic field in the Cretaceous (from Cretaceous rocks of Mongolia). Izv. Phys. Solid Earth 47 (9), 775–791.
Shcherbakova, V.V., Bakhmutov, V.G., Shcherbakov, V.P., Zhidkov, G.V., Shpyra, V.V., 2012. Palaeointensity and palaeomagnetic study of Cretaceous and Palaeocene rocks from Western Antarctica. Geophys. J. Int. 189, 204–228.
Shcherbakova, V.V., Zhidkova, G.V., Latyshevb, A.V., Scherbakov, V.P., 2013. Estimating the variations in paleointensity from the Siberian traps of Maymecha-Kotui and Norilsk regions. Izv. Phys. Solid Earth 49 (4), 488–504.
Shcherbakova, V.V., Zhidkov, G.V., Shcherbakov, V.P., Latyshev, A.V., Fetisova, A.M., 2015. Verifying the Mesozoic dipole low hypothesis by the Siberian trap data. Izv. Phys. Solid Earth 51 (3), 362–382.
Smirnov, A.V., Tarduno, J.A., 2003. Magnetic hysteresis monitoring of Cretaceous submarine basaltic glass during Thellier paleointensity experiments: evidence for alteration and attendant low field bias. Earth Planet. Sci. Lett. 206 (3–4), 571–585.
Tarduno, J.A., Cottrell, R.D., Smirnov, A.V., 2006. The paleomagnetism of single silicate crystals: recording geomagnetic field strength during mixed polarity intervals, superchrons, and inner core growth. Rev. Geohys. 44. http://dx.doi.org/10.1029/ 2005RG000189. RG1002.
Tauxe, L., Staudigel, H., 2004. Strength of the geomagnetic field in the Cretaceous Normal Superchron: new data from submarine basaltic glass of the Troodos Ophiolite. Geochem. Geophys. Geosyst. 5 (2). Art. No. Q02H06.
Tauxe, L., Yamazaki, T., 2007. Paleointensities. In: Kono, M. (Ed.), Geomagnetism. Elsevier, Amsterdam, pp. 510–563.
Tauxe, L., Gee, J.S., Steiner, M.B., Staudigel, H., 2013. Paleointensity results from the Jurassic: new constraints from submarine basaltic glasses of ODP Site 801C. Geochem. Geophys. Geosyst. 14 (10), 4718–4733.
Thellier, E., Thellier, O., 1959. Sur l'intensité du champ magnétique terrestre dans le passé historique et géologique. Ann. Geophys. 15, 285–376.
Thomas, D.N., Biggin, A.J., 2003. Does the Mesozoic dipole low really exist? EOS. Trans. Am. Geophys. Union 84 (11), 97–104.
Valet, J.P., 2003. Time variations in geomagnetic intensity. Rev. Geophys. 41, 1004. 1010.1029/2001RG000104.
Valet, J.-P., Brassart, J., Le Meur, I., Soler, V., Quidelleur, X., Tric, E., Gillot, P.-Y., 1996. Absolute paleointensity and magnetomineralogical changes. J. Geophys. Res. 101 (B11), 25029–25044. http://dx.doi.org/10.1029/96JB02115.
Valet, J.P., Meynadier, L., Guyodo, Y., 2005. Geomagnetic dipole strength and reversal rate over the past two million years. Nature 435, 802–805.
Walton, D., Snape, S., Rolph, T.C., Shaw, J., Share, J., 1996. Application of ferromagnetic resonance heating to palaeointensity determinations. Phys. Earth Planet. Inter. 94 (3–4), 183–186.
Wilson, R.L., 1961. The thermal demagnetization of natural magnetic moments in rocks. Geophys. J. R. Astron. Soc. 5 (1), 45–58.
Yu, Y., 2012. High-fidelity paleointensity determination from historic volcanoes in Japan. J. Geophys. Res. (Solid Earth) 117, B08101.
Yu, Y.J., Tauxe, L., 2005. Testing the IZZI protocol of geomagnetic field intensity determination. Geochem. Geophy. Geosyst. 6.
Zolotukhin, V.V., Al'mukhamedov, A.I., 1988. Traps of the Siberian platform. In: Macdougall, J.D. (Ed.), Continental Flood Basalts. Kluwer, Dordrecht, Netherlands, pp. 273–310.